JACS
JOURNAL OF THE AMERICAN CHEMICAL SOCIETY
Article
pubs.acs.org/JACS

Nanostructured Block-Random Copolymers with Tunable Magnetic Properties

Yongping Zha,[†,#] Hitesh D. Thaker,[†,#] Raghavendra R. Maddikeri,[†,#] Samuel P. Gido,[†] Mark T. Tuominen,[‡] and Gregory N. Tew*[,†]

[†]Department of Polymer Science and Engineering and [‡]Department of Physics, University of Massachusetts, Amherst, Massachusetts 01003, United States

Supporting Information

ABSTRACT: It was recently shown that block copolymers (BCPs) produced room-temperature ferromagnetic materials (RTFMs) due to their nanoscopic ordering and the cylindrical phase yielded the highest coercivity. Here, a series of metal-containing block-random copolymers composed of an alkyl-functionalized homo block (C_{16}) and a random block of cobalt complex- (Co) and ferrocene-functionalized (Fe) units was synthesized via ring-opening metathesis polymerization. Taking advantage of the block-random architecture, the influence of dipolar interactions on the magnetic properties of these nanostructured BCP materials was studied by varying the molar ratio of the Co units to the Fe units, while maintaining the cylindrical phase-separated morphology. DC magnetic measurements, including magnetization versus field, zero-field-cooled, and field-cooled, as well as AC susceptibility measurements showed that the magnetic properties of the nanostructured BCP materials could be easily tuned by diluting the cobalt density with Fe units in the cylindrical domains. Decreasing the cobalt density weakened the dipolar interactions of the cobalt nanoparticles, leading to the transition from a room temperature ferromagnetic (RTF) to a superparamagnetic material. These results confirmed that dipolar interactions of the cobalt nanoparticles within the phase-separated domains were responsible for the RTF properties of the nanostructured BCP materials.

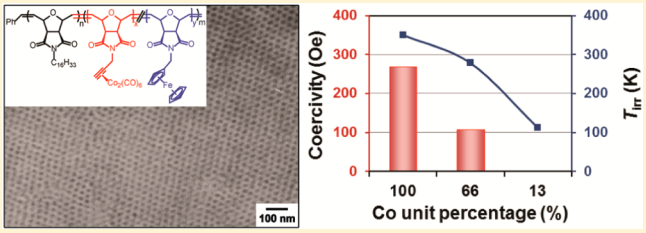

INTRODUCTION

Nanostructured materials, defined as having at least one dimension between 1 and 100 nm, have attracted intense research interest in recent years as they often exhibit novel and enhanced properties over their bulk counterparts.[1−4] Magnetic nanostructures are a particularly interesting class of materials for both scientific and technological reasons, with potential applications including high density information storage, spintronics, magnetic microelectromechanical systems, and biosensors.[5−9] Commercial magnetic nanostructure fabrication is dominated by conventional "top-down" techniques such as photolithography, electron-beam lithography, and X-ray lithography, most of which involve multiple steps and expensive instrumentation.[10] Alternatively, the self-assembly of block copolymers (BCPs) provides a cost-effective and rapid "bottom-up" approach that can outperform many "top-down" techniques in terms of feature size, periodic length scale, and simplicity.[11−13]

Recently, we reported a straightforward method to generate room-temperature ferromagnetic materials (RTFMs) from nanostructured BCPs with cobalt nanoparticles confined in one specific phase.[14] The results showed that the nanostructured morphologies were critical, and the room temperature ferromagnetic (RTF) behavior of the BCPs was thought to arise from enhanced dipolar interactions under nanoconfinement between the otherwise superparamagnetic cobalt nanoparticles. The dipolar interaction between magnetic elements is one of the main reasons why three-dimensional nanostructured materials can show improved magnetic properties over continuous bulk samples.[15] To date, most studies on dipolar interactions have been performed on ferrofluids,[16−18] magnetic colloids,[19−21] magnetic nanoparticles/nanowires incorporated into porous matrices,[5,22,23] and magnetic patterns prepared by lithography.[24] Those studies showed that dipolar interactions usually increase with increasing magnetic nanoparticle concentration, or decreasing distance between magnetic nanoelements.[16,22,25] This increase in dipolar interactions typically results in higher coercivity. It is thus reasonable to hypothesize that for our nanostructured BCPs, diluting the density of the cobalt nanoparticles in the domains will weaken the RTF behavior of the materials if it arises from the dipolar interactions of the cobalt nanoparticles under nanoconfinement.

In order to investigate the role of dipolar interactions on the magnetic properties of nanostructured BCP materials, it is desirable to vary the cobalt density in the domains while maintaining the phase-separated morphology, because the morphology also influences the magnetic properties.[14] This can be achieved by employing block-random copolymers, with

Received: May 30, 2012
Published: August 7, 2012

   dx.doi.org/10.1021/ja305249b | J. Am. Chem. Soc. 2012, 134, 14534−14541

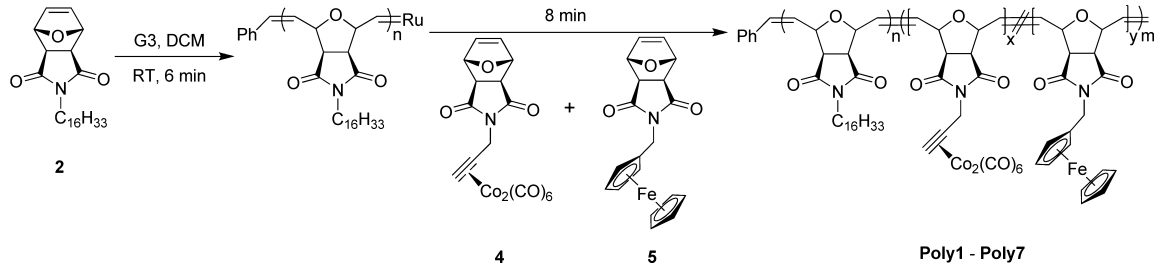

Figure 1. Synthesis of block-random copolymers **Poly1**−**Poly7**.

the general structure "A-*b*-(B-*r*-C)", where the first block is a homopolymer of monomer A and the second block is a random copolymer of monomers B and C.[26−28] The volume fraction of the random block would be held constant to maintain the same nanostructured morphology, while varying the cobalt density by changing the molar ratio of the cobalt-containing monomer to a diamagnetic comonomer in the random block. The living ring-opening metathesis polymerization (ROMP) enables the synthesis of such block-random copolymers, and has the potential to avoid common issues associated with traditional anionic polymerizations, where the differing monomer reactivity ratios often result in pronounced composition gradients along the random block.[29] Although living random copolymerizations by ROMP have been reported, there are very few detailed kinetic studies, and there is little characterization of ROMP-based block-random copolymers.[26,28,30,31]

In this report, a series of metal-containing block-random copolymers were synthesized by ROMP to study the influence of dipolar interactions on the magnetic properties of nanostructured BCP materials. The first block was an alkyl-functionalized (C_{16}) homopolymer, and the second block was a random copolymer consisting of cobalt complex- (Co) and ferrocene-functionalized (Fe) units. BCP materials containing the Co monomer were previously shown to generate RTFMs upon a simple heat treatment,[14] and the Fe monomer was chosen because ferrocene is diamagnetic (before and) after heat treatment but is still immiscible with the alkyl-functionalized block, maintaining phase separation. The copolymerization kinetics of the Co and Fe monomers were investigated, and the monomer reactivity ratios were calculated, confirming a random distribution of monomers along the Co-*r*-Fe block. Since the cylindrical morphology was previously shown to have the highest coercivity,[14] the volume fraction of the Co-*r*-Fe block was kept constant to ensure that the same cylindrical morphology was obtained for all of the block-random copolymers after phase separation. Meanwhile, the Co unit percentage in the Co-*r*-Fe block was systematically varied from 100% to 0%, which gradually reduced the cobalt density within the cylindrical domains. Magnetic measurements, including magnetization versus field (M−H), zero-field-cooled (ZFC), field-cooled (FC), and AC susceptibility, confirmed that the magnetic properties of these nanostructured block-random copolymers can be easily tuned by varying the cobalt density within the cylindrical domains.

RESULTS AND DISCUSSION

Monomer Synthesis. The same strained tricyclic monomer structure was used to provide similar polymerization rates and excellent initiation between blocks (Figure S1). The alkyl-functionalized monomer **2**[14] and the Co monomer **4**[32] were synthesized according to established procedures. Treatment of ferrocenemethanol with compound **1** afforded the Fe monomer **5** via Mitsunobu coupling (see Supporting Information for experimental details). The alkyl chain length of monomer **2** influences the microphase separation of the resulting BCPs, and a length of 16 (C_{16}) was chosen based on previous studies in which it exhibited the most well-defined microdomains.[14]

Polymer Synthesis. Block-random copolymers, **Poly1**−**Poly7**, with a C_{16} homo block and a Co-*r*-Fe block were synthesized by the stepwise polymerization of each block, as shown in Figure 1. First, the C_{16} homopolymer was prepared from monomer **2** by ROMP using the third generation Grubbs' catalyst (G3). When monomer **2** was completely consumed after 6 min, a mixture of monomers **4** and **5** was added to generate the block-random copolymers. The whole polymerization process required less than 15 min, and the monomer conversions for all of the polymers were ∼99%, highlighting the efficiency of ROMP.

To study the effect of the cobalt density in the cylindrical domains on the magnetic properties of the nanostructured BCP materials, a series of seven different block-random copolymers were synthesized. The composition details are listed in Table 1.

Table 1. Molecular Characteristics of Block-Random Copolymers Poly1−**Poly7**

polymer	M_n[a] (kDa)	M_w[a] (kDa)	PDI[a]	**4**: **5** (feed ratio)	x: y[b]
Poly1	82	89	1.09	80:20	76:24
Poly2	89	96	1.08	70:30	66:34
Poly3	85	92	1.08	60:40	54:46
Poly4	83	89	1.07	50:50	39:61
Poly5	90	95	1.06	40:60	32:68
Poly6	94	99	1.05	30:70	23:77
Poly7	100	107	1.07	20:80	13:87

[a]Determined by GPC in THF using refractive index (RI) detector, relative to polystyrene standards. [b]Molar ratio of the Co units (x) to the Fe units (y) in the random block calculated from ^{1}H NMR integration. The deviation from the feed ratio is likely due to error in the NMR integration, as the characteristic peak used for monomer **5** is close to peaks at 4.62−4.32 ppm, which are attributed to the protons from the oxanorbornene backbone and the methylene group in the Fe units (Figure S2).

All of the copolymers had similar molecular weights (MW) and narrow polydispersity indices (PDI). The molar ratio of the Co units (**4**) to the Fe units (**5**) in the Co-*r*-Fe block was varied from 80:20 to 20:80. Meanwhile, the volume fraction of the Co-*r*-Fe block was kept constant (0.23 ± 0.01) to ensure the same phase-separated morphology.

Polymer Characterization. The diblock architecture of the resulting copolymers was confirmed by gel permeation chromatography (GPC). Figure 2 shows representative GPC curves for the first C_{16} block and the final C_{16}-*b*-(Co-*r*-Fe)

dx.doi.org/10.1021/ja305249b | J. Am. Chem. Soc. 2012, 134, 14534−14541

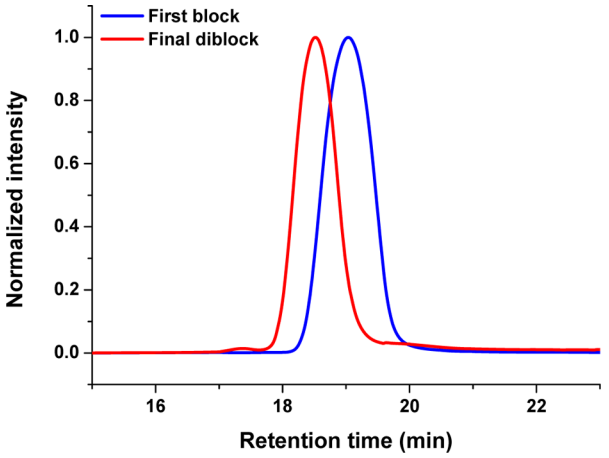

Figure 2. Representative GPC curves for the first block composed of the C_{16} homopolymer (blue) and the final C_{16}-*b*-(Co-*r*-Fe) diblock copolymer (**Poly5**) (red).

diblock copolymer (**Poly5**). A monomodal and narrow molecular weight distribution was preserved throughout. Only the cylindrical morphology was studied here, with a molar ratio of the C_{16} homo block to the Co-*r*-Fe block of 70:30, so the final diblock (red curve) is never completely shifted to higher molecular weight compared to the first block (blue curve). There is no evidence of remaining C_{16} homopolymer in the narrow monomodal curve for the final diblock, indicating efficient chain extension in the living polymerization.

The random copolymerization kinetics of the second Co-*r*-Fe block were investigated by ^{1}H NMR spectroscopy. Figure 3A shows the conversion as a function of time for the copolymerization of the Co monomer **4** (blue) and the Fe monomer **5** (red) for **Poly4** (feed ratio of **4** to **5** = 50/50). The conversions of the two monomers were almost identical at each time point, and both reached nearly 100% after 7 min. A living polymerization conducted isothermally is expected to be a first-order reaction,[33] and this should hold true for a random (gradient-free) copolymerization, as the relative monomer composition does not change with time.[31,34] Figure 3B shows the first-order time−conversion plots of monomer **4** (blue), monomer **5** (red), and the sum of **4** and **5** (black). The $[M]_0/[M]$ values ([M] denotes the monomer concentration) were obtained from the ordinate of Figure 3A. All three plots are linear, consistent with a polymerization that follows first-order kinetics with respect to the monomer. The monomer reactivity ratios, r_1 and r_2, for the living random copolymerization of monomers **4** and **5** were determined by the Fineman−Ross method[35] (Figure S3): r_1 = 0.89, r_2 = 1.67 (M_1 = monomer **4**, M_2 = monomer **5**). Although the r_1 and r_2 values calculated by this method should be treated with caution due to the steady-state assumption,[36] they indicate that the distribution of monomers **4** and **5** in the Co-*r*-Fe block is close to truly random.

Self-Assembly and Morphology Characterization. Solvent annealing was utilized to induce the self-assembly of the block-random copolymers, from a film formed by drop-casting a 10 wt% chloroform solution into a Teflon mold. Small angle X-ray scattering (SAXS) and transmission electron microscopy (TEM) were used to characterize the morphologies of the resulting samples. After solvent annealing, the SAXS profiles of the block-random copolymers all showed peaks corresponding to q^*, $\sqrt{3}q^*$, and $\sqrt{7}q^*$ (q^* denotes the primary scattering peak), indicating cylindrical morphologies. A representative SAXS profile for **Poly5** is shown in Figure 4A, and Figure 4B shows a representative bright field TEM image of the unstained solvent-annealed sample, providing clear evidence for the formation of well-defined phase-separated nanodomains. The dark contrast of the cylindrical domains is attributed to the presence of the heavy cobalt and iron atoms. The *d*-spacings were calculated from the SAXS data according to the equation $d = 2\pi/q^*$. The nanostructures obtained from **Poly1**−**Poly7** exhibited similar bulk periodicities, with *d*-spacing values ranging from 42 to 54 nm which is consistent with the diameters (~20 nm) of the metal-containing cylindrical domains obtained from the TEM images (Table 2).

Heat Treatment and Magnetic Properties. Our previous study showed that upon a simple heat treatment, the cobalt complex-containing diblock copolymers were converted to RTFMs while retaining their phase-separated morphology.[14] The thermal removal of carbonyl ligands from dicobalt hexacarbonyl metal complexes is well-known.[19,37−39] Thermogravimetric analysis (TGA) showed that the loss of the carbonyl moieties occurred between ~110−200 °C for the Co

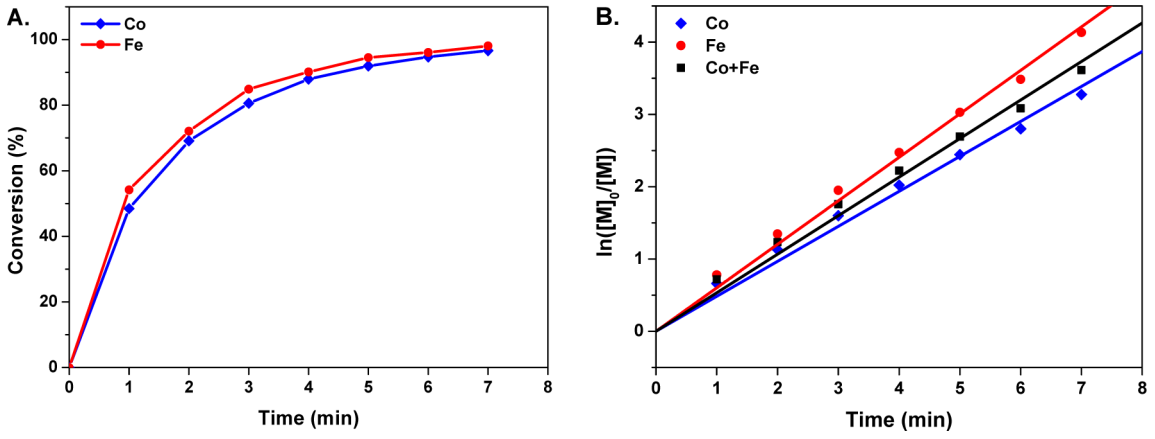

Figure 3. (A) Conversion of the cobalt complex-functionalized (Co) monomer **4** (blue) and the ferrocene-functionalized (Fe) monomer **5** (red) as a function of time for the random copolymerization of monomers **4** and **5**. (B) Linear fits of the first-order time−conversion relation of the Co monomer **4** (blue), Fe monomer **5** (red), and the sum of **4** and **5** (black). All the R^2 values for the linear fits are around 0.98. [M] denotes the monomer concentration.

dx.doi.org/10.1021/ja305249b | J. Am. Chem. Soc. 2012, 134, 14534−14541

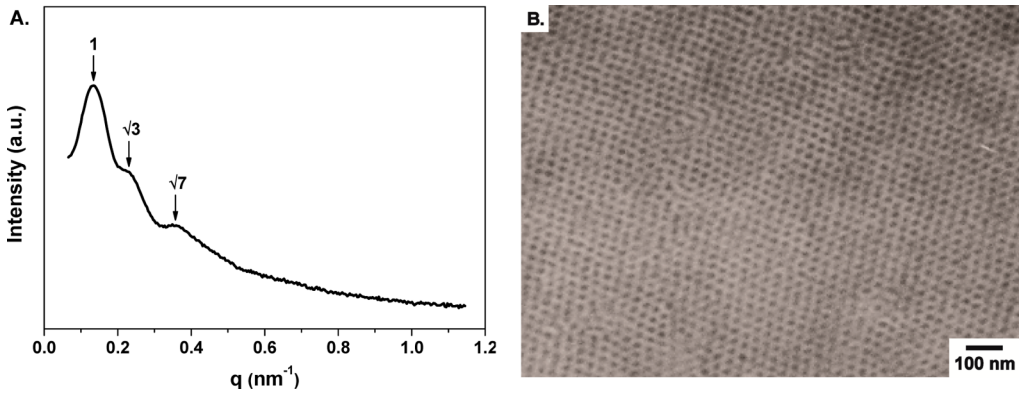

Figure 4. Representative (A) SAXS curve and (B) TEM micrograph of a block-random copolymer (**Poly5**) after solvent annealing in chloroform.

Table 2. Morphological Characteristics of Block-Random Copolymers Poly1−Poly7

polymer	f_{Co+Fe} [a]	Co (%) [b]	*d*-spacing (nm) [c]	d_{cyl} (nm) [d]
Poly1	0.24	76	47	20
Poly2	0.23	66	45	18
Poly3	0.23	54	45	21
Poly4	0.22	38	42	19
Poly5	0.22	32	47	20
Poly6	0.22	23	49	21
Poly7	0.22	13	54	19

[a]Volume fraction of the Co-*r*-Fe block (f_{Co+Fe}) calculated based on density data which were obtained by the gradient density column method. [b]Co unit percentage in the Co-*r*-Fe block calculated from ^{1}H NMR integration (Figure S2). [c]Bulk periodicity: $d = 2\pi/q^*$, where q^* is the primary scattering peak as determined by SAXS. [d]Diameter of the cylindrical domains (d_{cyl}) determined from the TEM images.

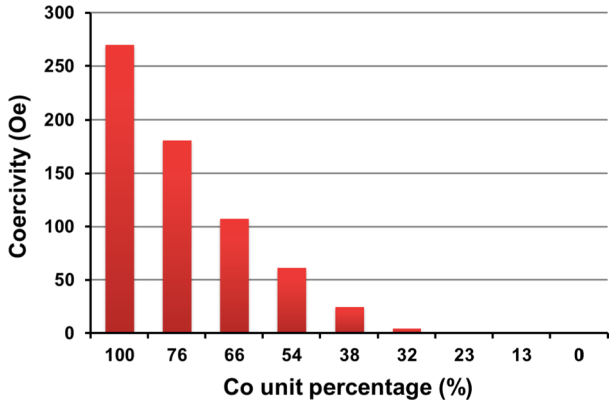

Figure 5. Impact of decreasing the Co unit percentage in the cylindrical domains on the coercivity of the nanostructured BCP materials.

homopolymer (Figure S4), and the weight loss indicated that about 94% of the carbonyl ligands were removed. By comparison, the C_{16} and Fe homopolymers showed no mass loss until above 350 °C. The samples were characterized by SAXS and TEM before and after heat treatment, and no significant changes to the morphology were observed (Figure S5).

***M*−*H* Measurement.** If the RTF behavior of the previously reported nanostructured BCP materials[14] was due to the enhanced dipolar interactions between the cobalt nanoparticles under nanoconfinement, decreasing the Co unit percentage should dilute the density of the cobalt nanoparticles in the domains and weaken the dipolar interactions between them, leading to lower coercivity values.[22,40] To investigate the effect of the cobalt density on the magnetic properties of the nanostructured BCP materials, the magnetization as a function of the applied field (*M*−*H*) was measured at room temperature by a superconducting quantum interference device (SQUID) for all of the thermally treated block-random copolymers. As shown in Figure S6, the saturation magnetization values decreased with decreasing Co unit percentage in the Co-*r*-Fe block (i.e., decreasing cobalt density in the cylindrical domains). The coercivity values at room temperature (in Oe) were obtained from the x-intercepts of the hysteresis loops and are plotted as a function of the Co unit percentage in the Co-*r*-Fe block in Figure 5. The C_{16}-*b*-Co (100% Co units) and C_{16}-*b*-Fe (0% Co units) diblock copolymers (with cylindrical morphologies) were also synthesized and characterized (see Supporting Information for experimental details), and the results are included in Figure 5. As the cobalt density in the cylindrical domains decreased, the coercivity of the nanostructured BCP materials decreased from greater than 250 Oe to almost zero, consistent with our hypothesis.

ZFC-FC Magnetization Measurement. The effect of the cobalt density within the cylindrical domains on the dipolar interactions between cobalt nanoparticles was further investigated by ZFC and FC magnetization measurements. Figure 6 shows the ZFC and FC curves for three different nanostructured BCP materials with (A) 100%, (B) 66%, and (C) 13% Co units in the cylindrical domains. The lower curves, labeled ZFC (black), were obtained by first cooling the samples from room temperature to 2 K in the absence of a magnetic field. A magnetic field of 100 Oe was then applied, and the magnetization was measured with increasing temperature from 0 to 350 K. The FC upper curves (red) were obtained in a similar way except that the samples were cooled in the measuring field (100 Oe).

A typical feature of magnetic nanoparticles is the irreversible magnetic behavior below a field-dependent blocking temperature (or irreversible temperature, T_{irr}).[41,42] The irreversible temperature indicates the onset of blocking for the largest particles in the magnetic materials.[43] Above T_{irr}, the ZFC and FC magnetization curves coincide, and the magnetic particles are superparamagnetic; below T_{irr}, the ZFC and FC magnetization curves separate, and the magnetic particles are ferromagnetic.[16,41] Experimentally, T_{irr} is defined as the temperature at which the difference between the ZFC and FC magnetizations is less than or equal to 1% of the FC

dx.doi.org/10.1021/ja305249b | J. Am. Chem. Soc. 2012, 134, 14534−14541

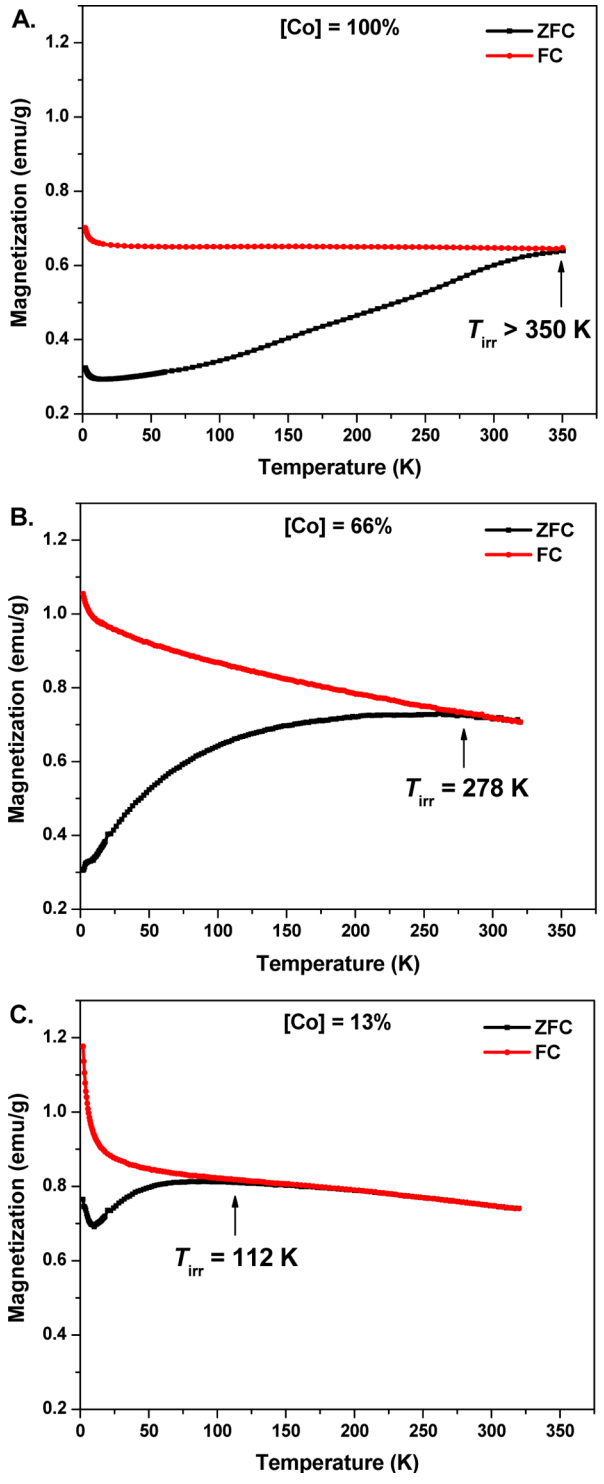

Figure 6. ZFC and FC magnetization curves under an applied field of 100 Oe for the nanostructured BCP materials with (A) 100%, (B) 66%, and (C) 13% Co units in the cylindrical domains. The irreversible temperatures (T_{irr}) for the samples are indicated on the plots.

magnetization value, i.e. $(M_{FC}(T_{irr}) - M_{ZFC}(T_{irr}))/M_{FC}(T_{irr}) \leq 0.01$.[42] A decrease in dipolar interactions is known to shift T_{irr} to a lower temperature because the dipolar interactions suppress thermal fluctuations of magnetic spins.[43]

This trend was also observed for our system, where the T_{irr} decreased with decreasing cobalt density. For the sample with 100% Co units in the cylindrical domains, the ZFC curve did not merge with the FC curve in the temperature range investigated, indicating that its T_{irr} was above 350 K (Figure 6A). By comparison, the ZFC curve for the 66% Co sample coincided with the FC curve at 278 K (Figure 6B) and a further decrease in T_{irr} to 112 K was observed for the 13% Co sample (Figure 6C). These results were consistent with those from the $M-H$ study where, as the dipolar interactions decreased with decreasing cobalt density, the coercivity decreased from 270 Oe (100% Co units) to nearly zero (0% Co units).

While the temperature at which the ZFC and FC curves converge indicates the blocking temperature for the largest particles in a system, a peak in the ZFC curve typically defines the average blocking temperature for a distribution of particles with different sizes.[44] As shown in Figure 6, the 100% Co sample exhibited a monotonic increase in the ZFC data with increasing temperature, indicating its average blocking temperature was also above 350 K. By contrast, the ZFC magnetizations of the 66% and 13% Co samples both increased at first and then decreased with increasing temperature. The peak temperatures of the 66% and 13% Co samples are ~260 and ~80 K, respectively. Like T_{irr}, a decrease in the average blocking temperature is usually observed as the dipolar interactions decrease.[22,44,45] In our system, as the cobalt density in the cylindrical domains decreased, the peak temperature of the ZFC magnetization curve decreased as well, indicating a decrease in the dipolar interactions, following the same trend observed for both coercivity and T_{irr}.

AC Susceptibility Measurement. Both the $M-H$ and ZFC-FC studies discussed above are direct current (DC) magnetic measurements, where a constant magnetic field was applied to determine the equilibrium value of the magnetization in the sample. Since the induced magnetic moment in the sample is time-dependent, an alternating current (AC) susceptibility measurement was performed to characterize the magnetization dynamics of the nanostructured BCP materials.[46] The AC susceptibility (χ) is the slope (dM/dH) of the $M-H$ magnetization curves. In an AC susceptibility measurement, the magnetization of a sample usually does not follow the DC magnetization curve due to magnetic dynamic effects in the sample, and the magnetization may lag behind the external field.[47] Thus, the AC susceptibility is composed of two components. The real component, χ', represents the component of the susceptibility that is in phase with the applied AC field; the imaginary component, χ'', represents the component that is out of phase.[48] Figure 7 shows the real and imaginary components, χ' and χ'', of the AC susceptibility as a function of temperature at various frequencies (30–10000 Hz) with an applied AC field of 5 Oe for the three nanostructured BCP materials with (A) 100%, (B) 66%, and (C) 13% Co units in the cylindrical domains.

For all three samples investigated, χ' decreased with increasing frequency, which is consistent with other interacting magnetic systems, like spin glasses.[49,50] However, χ' also increased with temperature and no peaks were observed in the temperature range investigated, which distinguishes the magnetic behavior of this system from that of canonical spin glass systems. The peak in χ' observed in spin glass systems is often interpreted as a phase transition between different magnetic states.[49,50] Although the lack of peaks in the χ' curves prevented the determination of the intrinsic relaxation times and energy barriers by an Arrhenius plot, χ' for the 100% Co sample (Figure 7A) increased continuously with temper-

dx.doi.org/10.1021/ja305249b | J. Am. Chem. Soc. 2012, 134, 14534–14541

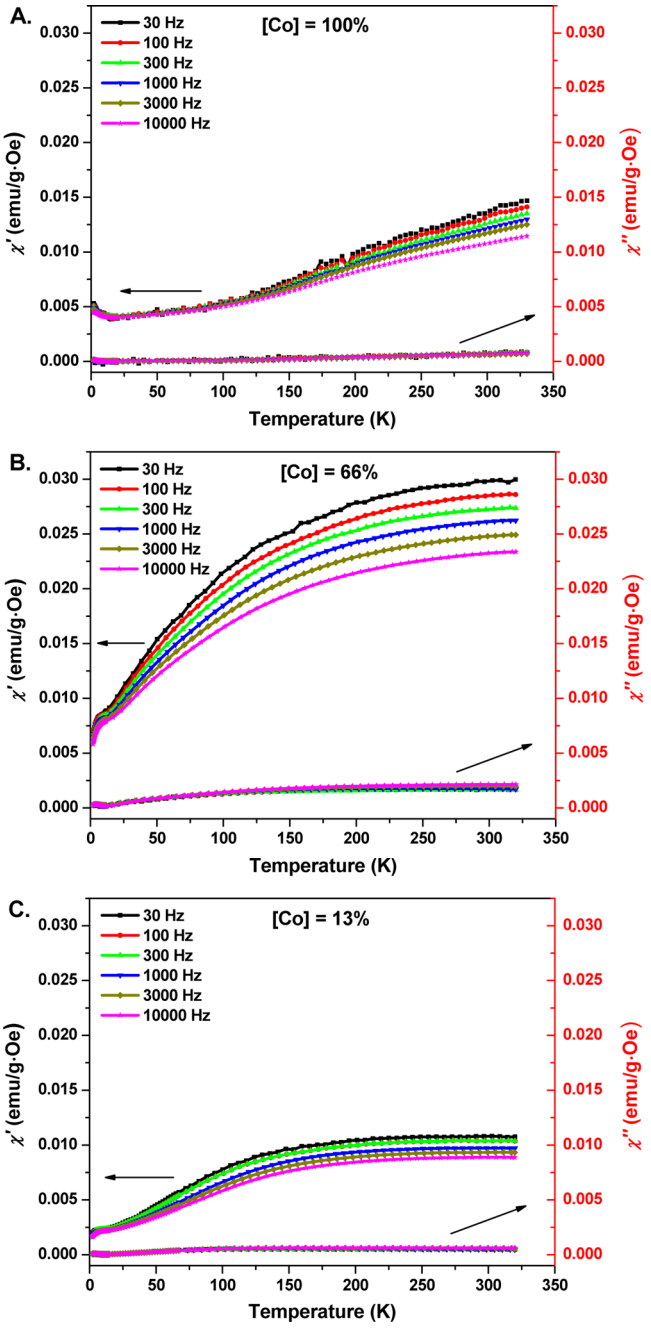

Figure 7. Temperature dependence of the in-phase and out-of-phase components, χ' and χ'', of the AC susceptibility, measured at various frequencies (30−10000 Hz) with an AC field of 5 Oe, for the nanostructured BCP materials with (A) 100%, (B) 66%, and (C) 13% Co units in the cylindrical domains.

ature, whereas saturation in χ' as a function of temperature was observed for the 66% and 13% Co samples (Figure 7B,C). Additionally, the saturation temperature for the 66% Co sample (~300 K) was clearly higher than that of the 13% Co sample (~225 K). It has been reported that with increasing dipolar interactions, the peak in the χ' curve shifts toward higher temperatures.[17,25] For our system, although no peak in χ' was observed, the χ' saturation temperatures followed the same trend. With decreasing cobalt density in the cylindrical domains, the dipolar interactions decreased. This was measured by a decrease in the χ' saturation temperature, which is in accordance with the results from the $M-H$ and ZFC-FC studies.

All of the magnetic measurements, including $M-H$, ZFC-FC, and AC susceptibility studies, are consistent with and support the idea that for our nanostructured BCP materials, diluting the density of cobalt units in the primary sequence weakens the RTF properties of the resulting materials due to interparticle dipolar interactions under nanoconfinement. As depicted in Figure 8, with decreasing cobalt density in the cylindrical

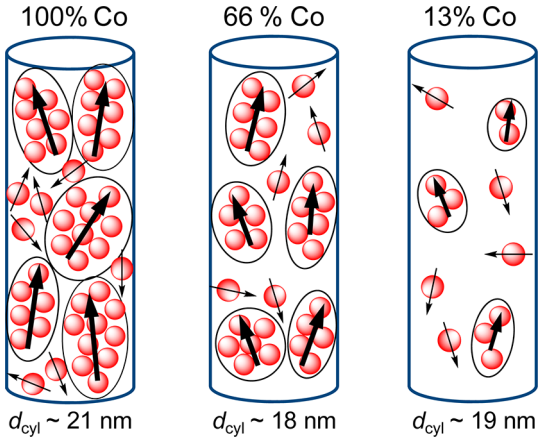

Figure 8. Schematic illustrating the decreased dipolar interactions between cobalt nanoparticles with decreasing cobalt density in the cylindrical domains. By controlling the number of cobalt units in the BCP primary sequence, the density of cobalt atoms in the nanocylinders is controlled. As the density decreases, the number of cobalt nanoparticles is decreased. This results in a larger average spacing between particles since the cylinder diameter is held constant. By increasing the average spacing between particles, the dipolar interactions between cobalt nanoparticles (represented by the ovals) become weaker,[22] leading to lower magnetic reversal temperatures.

domains, fewer cobalt nanoparticles are formed, and the collective magnetic spins resulting from dipolar interactions between cobalt nanoparticles become smaller, leading to weaker ferromagnetic properties. The formation of ~5 nm cobalt nanoparticles in the 100% Co sample (C_{16}-*b*-Co copolymer) was confirmed previously.[14] Given the whole collection of magnetic data, it seems safe to assume similar sized particles are formed by these new BCPs. Even if the particle size is smaller than 5 nm, they are still below the critical size for cobalt nanoparticles (10−12 nm);[51] therefore, the only way the samples reported here can be RTFMs is by having dipolar interactions among the particles assisted by the overall cylindrical shape anisotropy.[51] At the same time, it is unlikely (practically impossible) that nanoparticles are not formed at all as the cobalt density is decreased based on the ZFC-FC and AC measurements. For example, if no particles were present, there would be no dipolar interactions in the system, and the T_{irr} would be absent. However, even for the 13% Co sample which contains the least number of cobalt-containing monomers, T_{irr} is above 100 K, and the saturation temperature in the AC susceptibility measurement is above 200 K, indicating that there are dipolar interactions present in this system.

CONCLUSIONS

A straightforward synthetic approach based on ROMP was used to synthesize novel metal-containing block-random copolymers composed of a well-defined alkyl-functionalized (C_{16}) homo

dx.doi.org/10.1021/ja305249b | J. Am. Chem. Soc. 2012, 134, 14534−14541

block and a random block with cobalt complex- (Co) and ferrocene-functionalized (Fe) units. Kinetic studies showed that the random copolymerization of the Co monomer and the Fe monomer was a first-order reaction and close to "ideal". Holding the morphology constant and varying the molar ratio of the Co units to the Fe units in the random block showed that the cobalt density within the cylindrical domains directly impacted the RTF properties of the nanostructured BCP materials. This was consistent with the hypothesis that the RTF behavior of the nanostructured BCP materials was due to enhanced dipolar interactions under nanoconfinement between the otherwise superparamagnetic cobalt nanoparticles. This paper demonstrates the ability to systematically tune the magnetic properties by controlling the density of the magnetic species at the monomer, or primary sequence, level. These BCPs provide a new model system to study magnetic nanoparticles under confinement. The synthetic ease should allow them to be widely studied. Further functionalization with other metal species is expected to increase the range of properties. These RTFMs demonstrate the concept that learning to build chemically rich polymers will lead to new and unexpected materials.

EXPERIMENTAL SECTION

All experimental procedures, including the synthesis of monomers and block-random copolymers, as well as detailed information about characterization techniques are included in the Supporting Information.

ASSOCIATED CONTENT

Supporting Information

Experimental procedures and Figures S1–S6 (Fineman–Ross plot, TGA, SAXS, TEM, and *M*–*H* measurements). This material is available free of charge via the Internet at http://pubs.acs.org.

AUTHOR INFORMATION

Corresponding Author

tew@mail.pse.umass.edu

Author Contributions

[#]Y.Z., H.D.T., and R.R.M. contributed equally to this article.

Notes

The authors declare no competing financial interest.

ACKNOWLEDGMENTS

We acknowledge the support of ARO (Grant W911NF-09-1-0373) for funding this work. We are also grateful for the support of the Materials Research Science and Engineering Center (MRSEC) at the University of Massachusetts Amherst (DMR-0820506). Mass spectral data were obtained at the University of Massachusetts Mass Spectrometry Facility, which is supported, in part, by the National Science Foundation. The authors thank Dr. Abhigyan Som and Ms. Melissa A. Lackey for assisting manuscript preparation.

REFERENCES

(1) Edelstein, A. S.; Cammarata, R. C. *Nanomaterials: Synthesis, Properties, and Applications*, 1st ed.; Taylor & Francis Group: New York, NY, 1996.

(2) Alivisatos, A. P.; Barbara, P. F.; Castleman, A. W.; Chang, J.; Dixon, D. A.; Klein, M. L.; McLendon, G. L.; Miller, J. S.; Ratner, M. A.; Rossky, P. J.; Stupp, S. I.; Thompson, M. E. *Adv. Mater.* **1998**, *10*, 1297.

(3) Xia, Y. N.; Yang, P. D.; Sun, Y. G.; Wu, Y. Y.; Mayers, B.; Gates, B.; Yin, Y. D.; Kim, F.; Yan, H. Q. *Adv. Mater.* **2003**, *15*, 353.

(4) Thiaville, A.; Miltat, J. *Science* **1999**, *284*, 1939.

(5) Thurn-Albrecht, T.; Schotter, J.; Kästle, G. A.; Emley, N.; Shibauchi, T.; Krusin-Elbaum, L.; Guarini, K.; Black, C. T.; Tuominen, M. T.; Russell, T. P. *Science* **2000**, *290*, 2126.

(6) Prinz, G. A. *Science* **1998**, *282*, 1660.

(7) Wolf, S. A.; Awschalom, D. D.; Buhrman, R. A.; Daughton, J. M.; von Molnár, S.; Roukes, M. L.; Chtchelkanova, A. Y.; Treger, D. M. *Science* **2001**, *294*, 1488.

(8) Myung, N. V.; Park, D. Y.; Yoo, B. Y.; Sumodjo, P. T. A. *J. Magn. Magn. Mater.* **2003**, *265*, 189.

(9) Edelstein, R. L.; Tamanaha, C. R.; Sheehan, P. E.; Miller, M. M.; Baselt, D. R.; Whitman, L. J.; Colton, R. J. *Biosens. Bioelectron.* **2000**, *14*, 805.

(10) Wallraff, G. M.; Hinsberg, W. D. *Chem. Rev.* **1999**, *99*, 1801.

(11) Hawker, C. J.; Russell, T. P. *MRS Bull.* **2005**, *30*, 952.

(12) Bang, J.; Kim, S. H.; Drockenmuller, E.; Misner, M. J.; Russell, T. P.; Hawker, C. J. *J. Am. Chem. Soc.* **2006**, *128*, 7622.

(13) Rider, D. A.; Liu, K.; Eloi, J. C.; Vanderark, L.; Yang, L.; Wang, J. Y.; Grozea, D.; Lu, Z. H.; Russell, T. P.; Manners, I. *ACS Nano* **2008**, *2*, 263.

(14) Al-Badri, Z. M.; Maddikeri, R. R.; Zha, Y.; Thaker, H. D.; Dobriyal, P.; Shunmugam, R.; Russell, T. P.; Tew, G. N. *Nat. Commun.* **2011**, *2*, 482.

(15) Hehn, M.; Ounadjela, K.; Bucher, J. P.; Rousseaux, F.; Decanini, D.; Bartenlian, B.; Chappert, C. *Science* **1996**, *272*, 1782.

(16) Luo, W. L.; Nagel, S. R.; Rosenbaum, T. F.; Rosensweig, R. E. *Phys. Rev. Lett.* **1991**, *67*, 2721.

(17) Jonsson, T.; Nordblad, P.; Svedlindh, P. *Phys. Rev. B* **1998**, *57*, 497.

(18) Klokkenburg, M.; Vonk, C.; Claesson, E. M.; Meeldijk, J. D.; Erne, B. H.; Philipse, A. P. *J. Am. Chem. Soc.* **2004**, *126*, 16706.

(19) Korth, B. D.; Keng, P.; Shim, I.; Bowles, S. E.; Tang, C.; Kowalewski, T.; Nebesny, K. W.; Pyun, J. *J. Am. Chem. Soc.* **2006**, *128*, 6562.

(20) Benkoski, J. J.; Bowles, S. E.; Korth, B. D.; Jones, R. L.; Douglas, J. F.; Karim, A.; Pyun, J. *J. Am. Chem. Soc.* **2007**, *129*, 6291.

(21) Kim, B. Y.; Shim, I. B.; Araci, Z. O.; Saavedra, S. S.; Monti, O. L. A.; Armstrong, N. R.; Sahoo, R.; Srivastava, D. N.; Pyun, J. *J. Am. Chem. Soc.* **2010**, *132*, 3234.

(22) Gross, A. F.; Diehl, M. R.; Beverly, K. C.; Richman, E. K.; Tolbert, S. H. *J. Phys. Chem. B* **2003**, *107*, 5475.

(23) Cao, H. Q.; Xu, Z.; Sang, H.; Sheng, D.; Tie, C. Y. *Adv. Mater.* **2001**, *13*, 121.

(24) Cowburn, R. P. *J. Phys. D: Appl. Phys.* **2000**, *33*, R1.

(25) Jonsson, T.; Mattsson, J.; Djurberg, C.; Khan, F. A.; Nordblad, P.; Svedlindh, P. *Phys. Rev. Lett.* **1995**, *75*, 4138.

(26) Aamer, K. A.; Tew, G. N. *Macromolecules* **2004**, *37*, 1990.

(27) Quinn, J. D.; Register, R. A. *J. Polym. Sci., Part B: Polym. Phys.* **2009**, *47*, 2106.

(28) Sandholzer, M.; Slugovc, C. *Macromol. Chem. Phys.* **2009**, *210*, 651.

(29) Morton, M. *Anionic Polymerization: Principles and Practice*; Academic Press: New York, 1983.

(30) Xia, Y.; Olsen, B. D.; Kornfield, J. A.; Grubbs, R. H. *J. Am. Chem. Soc.* **2009**, *131*, 18525.

(31) Conrad, R. M.; Grubbs, R. H. *Angew. Chem., Int. Ed.* **2009**, *48*, 8328.

(32) Al-Badri, Z. M.; Tew, G. N. *Macromolecules* **2008**, *41*, 4173.

(33) Müller, A. H. E.; Matyjaszewski, K. *Controlled and Living Polymerizations: From Mechanisms to Applications*; Wiley-VCH: Weinheim, 2009.

(34) Beckingham, B. S.; Register, R. A. *Macromolecules* **2011**, *44*, 4313.

(35) Fineman, M.; Ross, S. D. *J. Polym. Sci.* **1950**, *5*, 259.

(36) Meyer, V. E.; Lowry, G. G. *J. Polym. Sci., Part A* **1965**, *3*, 2843.

(37) Puntes, V. F.; Zanchet, D.; Erdonmez, C. K.; Alivisatos, A. P. *J. Am. Chem. Soc.* **2002**, *124*, 12874.

(38) Clendenning, S. B.; Aouba, S.; Rayat, M. S.; Grozea, D.; Sorge, J. B.; Brodersen, P. M.; Sodhi, R. N. S.; Lu, Z. H.; Yip, C. M.; Freeman, M. R.; Ruda, H. E.; Manners, I. *Adv. Mater.* **2004**, *16*, 215.
(39) Scholz, S.; Leech, P. J.; Englert, B. C.; Sommer, W.; Weck, M.; Bunz, U. H. F. *Adv. Mater.* **2005**, *17*, 1052.
(40) Zhang, L.; Manthiram, A. *Phys. Rev. B* **1996**, *54*, 3462.
(41) Prozorov, R.; Yeshurun, Y.; Prozorov, T.; Gedanken, A. *Phys. Rev. B* **1999**, *59*, 6956.
(42) Zhang, P.; Zuo, F.; Urban, F. K., III; Khabari, A.; Griffiths, P.; Hosseini-Tehrani, A. *J. Magn. Magn. Mater.* **2001**, *225*, 337.
(43) Hanson, M.; Johansson, C.; Pedersen, M. S.; Mørup, S. *J. Phys.: Condens. Matter* **1995**, *7*, 9269.
(44) Zhang, Y. D.; Budnick, J. I.; Hines, W. A.; Chien, C. L.; Xiao, J. Q. *Appl. Phys. Lett.* **1998**, *72*, 2053.
(45) Sun, S. H.; Murray, C. B. *J. Appl. Phys.* **1999**, *85*, 4325.
(46) Das, M. P. *Condensed Matter: New Research*, 1st ed.; Nova Science Publishers, Inc.: New York, NY, 2007.
(47) Tran, L. K. *Superconductivity, Magnetism and Magnets*; Nova Science Publishers, Inc.: New York, NY, 2006.
(48) Giapintzakis, J.; Neiman, R. L.; Ginsberg, D. M.; Kirk, M. A. *Phys. Rev. B* **1994**, *50*, 16001.
(49) Mydosh, J. A. *J. Magn. Magn. Mater.* **1996**, *157*, 606.
(50) Vincent, E.; Yuan, Y.; Hammann, J.; Hurdequint, H.; Guevara, F. *J. Magn. Magn. Mater.* **1996**, *161*, 209.
(51) Jun, Y. W.; Seo, J. W.; Cheon, J. W. *Acc. Chem. Res.* **2008**, *41*, 179.